Article

Joint UAV Trajectory Planning and LEO Satellite Selection for Data Offloading in Space-Air-Ground Integrated Networks

Tie Liu [1] (ORCID)**, Firstname Lastname [2] and Firstname Lastname [2],***

[1] Affiliation 1; e-mail@e-mail.com
[2] Affiliation 2; e-mail@e-mail.com
* Correspondence: e-mail@e-mail.com; Tel.: (optional; include country code; if there are multiple corresponding authors, add author initials) +xx-xxxx-xxx-xxxx (F.L.)

Abstract

The rapid advancement of low Earth orbit (LEO) satellite constellations and unmanned aerial vehicles (UAVs) has positioned space–air–ground integrated networks as a key enabler of large-scale IoT services. However, ensuring reliable end-to-end operation remains challenging due to heterogeneous IoT–UAV link conditions and rapidly varying satellite visibility. This work proposes a two-stage optimization framework that jointly minimizes UAV energy consumption during IoT data acquisition and ensures stable UAV–LEO offloading through a demand-aware satellite association strategy. The first stage combines gradient-based refinement with combinatorial path optimization, while the second stage triggers handover only when the remaining offloading demand cannot be met. Simulation results show that the framework reduces UAV energy consumption by over 20% and shortens flight distance by more than 30% in dense deployments. For satellite offloading, the demand-aware strategy requires only 2–3 handovers—versus 7–9 under greedy selection—and lowers packet loss from 0.47–0.60% to 0.13–0.20%. By improving both stages simultaneously, the framework achieves consistent end-to-end performance gains across varying IoT densities and constellation sizes, demonstrating its practicality for future SAGIN deployments.

Keywords: SAGIN, UAV-assisted IoT, LEO satellite communications, trajectory planning, satellite handover, mobility management.

1. Introduction

Although Internet of Things (IoT) devices have been widely deployed in applications such as environmental monitoring, intelligent transportation and industrial sensing[1][2]. Terrestrial networks often fail to provide reliable coverage for large scale and spatially distributed IoT deployments, particularly when devices are located beyond the effective range of existing infrastructure or in environments with highly variable link conditions[3][4]. In this context, space–air–ground integrated networks (SAGINs) have emerged as a promising architecture: unmanned aerial vehicles (UAVs) act as flexible aerial aggregators for ground IoT data, while low Earth orbit (LEO) satellites provide wide area connectivity for offloading the aggregated data to the space segment[5][6].

However, the efficiency of IoT devices data acquisition is strongly influenced by the UAV platform's mobility strategy[7][8]. Optimizing the flight path and determining appropriate hovering points enable UAVs to better align with the spatial distribution of ground devices[9][10]. Another fundamental challenge arises from the limited spectrum resources

on UAVs, which restrict the number of IoT devices that can be served simultaneously and lead to low spectral efficiency under conventional orthogonal access schemes.

Motivated by these challenges, numerous studies have investigated UAVs for IoT data collection[11][12]. The work in [13] uses fractional programming and block coordinate descent to jointly optimize UAV trajectory and continuous communication resources. It relies on multiple access with unit bandwidth and does not consider spectrum domain allocation strategies. In [14], a hierarchical framework is introduced to uniformly optimize the total energy consumption across UAV collection of IoTs Data and satellite selection for offloading to LEO satellites. The work focuses primarily on the structural design of the framework, and the optimization aimed at improving performance is not further developed.

Beyond data acquisition on the ground side, another line of work focuses on how UAVs deliver the collected information to satellites[15][16][17]. The delivery of the collected information to LEO satellites introduces another layer of complexity, as the UAV must decide how to offload data under temporally dynamic link quality, limited communication resources, and dynamic satellite visibility. The authors in [18] investigates the computational tasks and resource allocation in a UAV assisted LEO satellite network,taking into account satellite computing resources and device task volumes. The study in [19] employs a Proximal Policy Optimization (PPO) driven reinforcement learning framework that intelligently adapts UAV placement and computation offloading strategies.

While recent studies have examined data collection through UAVs and task offloading toward LEO satellites, these efforts are often these efforts have often been pursued as independent performance metrics. Although a hierarchical framework have been proposed, its underlying optimization issues have yet to be thoroughly explored. In particular, existing approaches rarely provide designs guided by system performance for collecting data with improved energy efficiency or for maintaining stable satellite association under dynamic visibility. These constraints have prompted us to propose a structured framework that simultaneously optimizes both phases of the uplink process and thoroughly enhances the framework's performance.

The main contributions of this work are summarized as follows:

- A structured uplink framework is developed for data delivery in SAGIN environments. The framework separates the process of collecting data from IoT devices and the process of delivering the collected information to LEO satellites, and it formalizes the optimization objectives of both stages in a consistent manner.
- An algorithm is developed for the data collection phase to improve energy efficiency by jointly optimizing multiple access device pairing, transmission power, hovering positions, and the movement of UAVs. The continuous variables, such as hovering locations, are refined using gradient information through the Adam optimizer, while the visiting sequence of hovering points is improved by a 2-opt procedure that removes redundant detours in the trajectory. This combined approach reduces both flight distance and total energy consumption.
- A selection strategy driven by transmission demand is designed for the offloading phase to enhance the quality of uplink transmission under dynamic satellite visibility. The strategy maintains stable connectivity by triggering satellite switching only when residual transmission requirements are not met, thereby minimizing interruptions and packet loss.
- Extensive simulations are conducted to evaluate the proposed framework. The results show consistent gains in energy consumption, trajectory performance, and offloading stability over baseline methods, indicating that the two phase design provides effective improvements when integrated into a complete uplink procedure.

The remainder of this paper is organized as follows. Section 2 introduces the system model and formulates the optimization problems for the two phases of the uplink process. Section 3 presents the proposed methods for data collection and satellite selection. Section 4 provides simulation results and evaluates the performance of the proposed framework. Section 5 discusses the insights and implications revealed by the numerical analyses. Finally, Section 6 concludes the paper.

2. Materials and Methods

As shown in Figure 1, the considered SAGIN consists of **U** UAVs denoted by $\mathcal{U} = 1, 2, \ldots, U$ and **S** LEO satellites indicated by $\mathcal{S} = 1, 2, \ldots, S$. In addition, **K** IoT devices randomly scattered on the ground are represented as $\mathcal{K} = 1, 2, \ldots, K$. Due to the limited computational capabilities of IoT terminals, the data they collect must be uploaded to LEO satellites for further processing. However, constrained by their own energy and transmission power limitations, IoT devices struggle to communicate directly with these satellites. To address this issue, UAVs are employed as aerial base stations to support data aggregation and forwarding within the designated area. Under this architecture, the data uploading procedure is organized into two phases. In the first phase, the UAV follows a predetermined trajectory and visits a sequence of hovering locations to collect data generated by ground IoT devices, after which it returns to its initial position. In the second phase, once back at the initial position, the UAV remains stationary and selects an appropriate LEO satellite to execute computational offloading tasks.
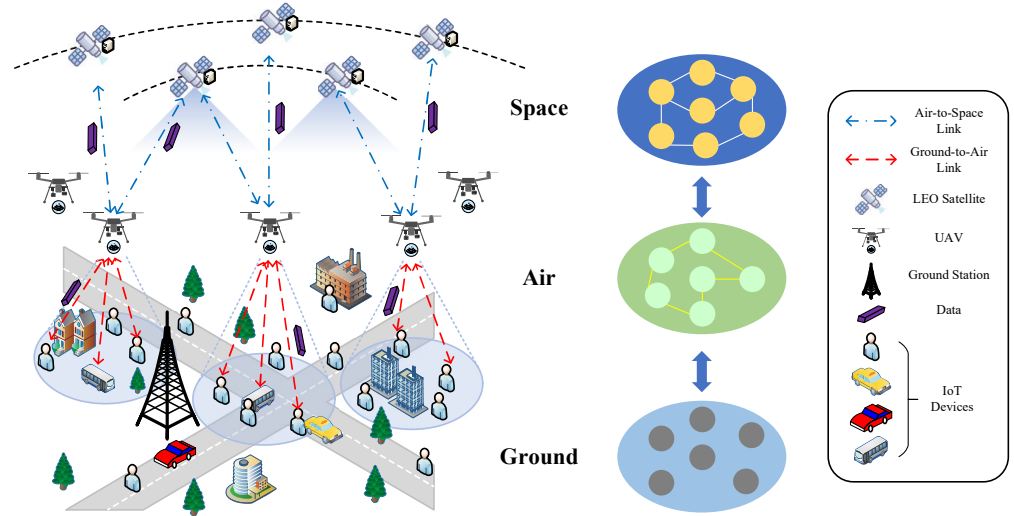

Figure 1. Illustration of the uplink communication procedure in SAGIN, where UAVs act as aerial aggregators to collect data from spatially distributed IoT devices and subsequently offload the aggregated data to LEO satellites.

2.1. Data Collection from IoT to UAV

During the data uploading phase between IoT devices and UAVs, Non-Orthogonal Multiple Access (NOMA) is employed to enhance spectrum efficiency and transmission performance. Specifically, it is assumed that within a defined spatial range, any two IoT devices may form a cooperative pair and transmit their uplink data simultaneously to the UAV using the NOMA mechanism. For devices that do not satisfy the pairing conditions or fail to form a valid pair, Orthogonal Frequency Division Multiple Access (OFDMA) is used to support independent data transmission.

A three-dimensional Cartesian coordinate system is adopted to describe the spatial distribution of UAVs and IoT devices. The IoT devices are randomly deployed on the
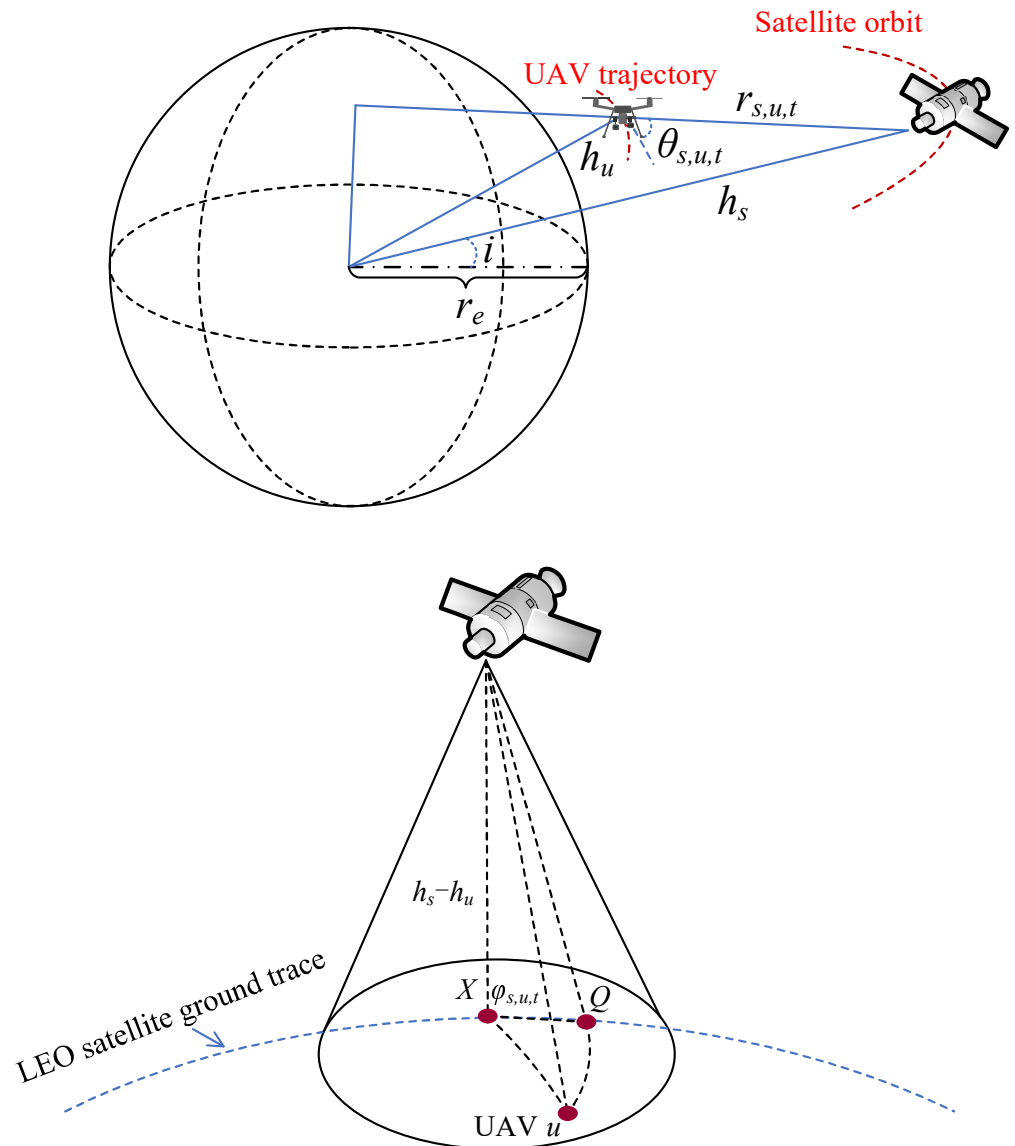
Figure 2. Geometric illustration of the UAV–LEO satellite link, including the satellite orbit, UAV position, Earth curvature, slant-range distance, and elevation angle, which together characterize the air-to-space propagation model employed in this study.

ground plane, and the location of the k-th device is represented by $\mathbf{q}_k = (x_k, y_k, 0)$. Each UAV maintains a constant altitude h_u; hence, its position at the n-th hovering point is given by $\mathbf{q}_u(n) = (x_u(n), y_u(n), h_u)$. Owing to the elevated UAV altitude and the predominantly unobstructed propagation conditions, the wireless links between IoT devices and UAVs are primarily characterized by line-of-sight (LoS) propagation. Accordingly, the channel gain between IoT device k and its associated UAV is modeled as

$$d_k(n) = \sqrt{h_u^2 + (x_u(n) - x_k)^2 + (y_u(n) - y_k)^2}, \qquad G_k = \frac{\beta_0}{d_k(n)^2}. \tag{1}$$

where β_0 is the channel gain measured at the reference distance $r_0 = 1\,\text{m}$.

Let $\mathcal{P}$ denote the set of all feasible transmission pairs, where each pair $p \in \mathcal{P}$ consists of either (i) two IoT devices forming a NOMA cluster or (ii) a single device operating in OFDMA mode. A binary decision variable $\delta_p \in \{0, 1\}$ is introduced to indicate whether pair p is activated. To ensure that each IoT device participates in at most one transmission pair, the following constraint is imposed

$$\sum_{p \in \mathcal{P}: k \in p} \delta_p \leq 1, \qquad \forall k \in \mathcal{K}. \tag{2}$$

Given the pairing configuration, the received signal-to-interference-plus-noise ratio (SINR) of IoT device k can be expressed as

$$\text{SINR}_k = \frac{p_k G_k}{\displaystyle\sum_{p \in \mathcal{P}: k \in p} \delta_p \sum_{\substack{j \in p \\ j \neq k}} p_j G_j + \sigma_{iu}^2}, \tag{3}$$

where p_k is the transmit power of device k, and σ_{iu}^2 denotes the receiver noise power. The intra-pair interference term $\sum_{j \in p, j \neq k} p_j G_j$ appears only when the activated pair p contains two devices. For NOMA pairs, the decoding order is determined by the channel gains, followingthe conventional successive interference cancellation (SIC) procedure.

Given the SINR expression, the achievable uplink data rate of device k is

$$d_k = B_{iu} \log_2(1 + \text{SINR}_k), \tag{4}$$

where B_{iu} denotes the bandwidth allocated to UAV communications. For a task of size D_k, the corresponding uplink transmission delay is

$$T_k^{\text{tr}} = \frac{D_k}{d_k}. \tag{5}$$

After determining the trajectory of each UAV, a fixed visiting sequence is imposed to ensure that all NOMA clusters and singleton IoT devices are sequentially served. The trajectory of UAV u is denoted by the ordered set

$$\{\mathbf{q}_u(0), \mathbf{q}_u(1), \ldots, \mathbf{q}_u(N_u)\}, \tag{6}$$

where N_u represents the number of hovering waypoints assigned to UAV u. Accordingly, the total flight path length of UAV u throughout the mission is expressed as

$$L_u = \sum_{n=0}^{N_u - 1} \|\mathbf{q}_u(n+1) - \mathbf{q}_u(n)\|_2, \tag{7}$$

which captures the cumulative Euclidean distance traveled between consecutive hovering waypoints.

Given a constant flight speed v_f, the total flight time required by UAV u is calculated as

$$T_u^{\text{fly}} = \frac{L_u}{v_f}, \tag{8}$$

where L_u denotes the total flight path length of UAV u. This expression follows directly from the definition of time as distance divided by speed under constant-velocity motion.

During the data collection phase, each UAV hovers at designated waypoints to receive data from the associated IoT devices. The hovering duration of UAV u depends on the transmission times of all active NOMA pairs and is given by

$$T_u^{\text{hov}} = \sum_{p \in P} \delta_p \max_{k \in p} \frac{D_k}{d_k}, \tag{9}$$

where δ_p indicates whether pair p is assigned to UAV u, and the term $\max_{k \in p} \frac{D_k}{d_k}$ denotes the transmission time of pair p, dominated by the device with the longest individual transmission time.

During this phase, the energy consumption of UAV u consists of both hovering energy and flight related energy. Accordingly, the total energy consumption is given by

$$E_{\text{total}} = \sum_{u=1}^{U} \left(P_h T_u^{\text{hov}} + P_f T_u^{\text{fly}} \right), \tag{10}$$

where P_h and P_f denote the hovering power and flight power of the UAVs, respectively, and T_u^{fly} is the flight time of UAV u as defined earlier.

2.2. Data Offloading from UAV to LEO

After completing data collection from all IoT devices, each UAV obtains the position information of all visible LEO satellites and selects the satellite that can satisfy its offloading requirements.To represent the computation offloading decision, a binary association variable $\beta_{s,u,t} \in \{0,1\}$ is introduced, where $\beta_{s,u,t} = 1$ indicates that UAV u offloads its computation to satellite s at time slot t.

The large scale channel between UAV u and LEO satellite s is modeled using the free space path loss model, given in dB by

$$L_{s,u,t}^{\text{fs}}(\text{dB}) = 92.45 + 20 \log_{10}(r_{s,u,t}) + 20 \log_{10}(f_s), \tag{11}$$

where f_s denotes the carrier frequency of satellite s in GHz. The line-of-sight distance $r_{s,u,t}$ is obtained from the geometric relationship illustrated in Fig. 2, given by

$$r_{s,u,t} = \sqrt{(r_e + h_s)^2 + (r_e + h_u)^2 - 2(r_e + h_s)(r_e + h_u) \cos \theta_{s,u,t}}, \tag{12}$$

where r_e denotes the Earth radius, and h_u and h_s are the altitudes of the UAV and the LEO satellite, respectively.

The elevation angle $\theta_{s,u,t}$ between UAV u and satellite s is obtained from the satellite–UAV geometry shown in Fig. 2 and is expressed as

$$\theta_{s,u,t} = \arctan\left(\frac{h_s - h_u}{d_{\text{ground},s,u,t}} \right), \qquad d_{\text{ground},s,u,t} = r_e \phi_{s,u,t}, \tag{13}$$

where $d_{\text{ground},s,u,t}$ denotes the ground-projected distance between UAV u and the sub-satellite point, and $\phi_{s,u,t}$ is the corresponding central angle on the Earth's surface. Following [20], the central angle evolves over time as

$$\phi_{s,u,t} = (\omega_E \cos i - \omega_S)(t - t_0) + \phi_{s,u,t_0}, \tag{14}$$

where ω_E and ω_S denote the angular velocities of the Earth and satellite orbit, respectively, i is the orbital inclination, t_0 is the time instant when the satellite becomes visible to the UAV, and ϕ_{s,u,t_0} is the initial central angle.

The received power at LEO satellite s from UAV u at time t is given by

$$P_{s,u,t}^{\text{re}} = P_{tr} G_{tr} G_{re} G_{s,u,t}^{\text{lin}}, \tag{15}$$

where P_{tr} denotes the UAV transmit power, G_{tr} and G_{re} are the transmit and receive antenna gains, and $G_{s,u,t}^{\text{lin}}$ is the large-scale channel gain derived from the free-space path-loss model described in equation (11).

Based on the received power, the achievable uplink data rate from UAV u to satellite s at time t follows the Shannon capacity expression

$$d_{s,u,t} = B_{su} \log_2\left(1 + \frac{P_{s,u,t}^{\text{re}}}{\sigma_{su}^2}\right), \tag{16}$$

where B_{su} is the allocated bandwidth of the UAV–LEO link and $\sigma_{su}^2 = N_0 B_{su}$ denotes the receiver noise power. Let $x_{s,u,t} \in \{0,1\}$ denote the satellite association decision, where $x_{s,u,t} = 1$ indicates that UAV u is connected to satellite s at time t.

To account for unnecessary satellite switching, the handover indicator is defined as

$$h_{u,t} = \frac{1}{2} \sum_{s=1}^{S} |x_{s,u,t} - x_{s,u,t-1}|. \tag{17}$$

2.3. Problem Formulation

To minimize the total energy consumption in the first-stage IoT–UAV data collection process, we jointly optimize the pair-selection variables $\delta = \{\delta_p \mid p \in P\}$, the transmit-power allocation of IoT devices $\mathbf{p} = \{p_k \mid k \in K\}$, and the UAV hovering positions and visiting order $\mathbf{q} = \{\mathbf{q}_u(n) \mid u \in U\}$. The optimization problem is formulated as

$$\mathcal{P}_1 : \min_{\delta, \mathbf{p}, \mathbf{q}} \quad \sum_{u=1}^{U} \left(P_h \sum_{p \in P_u} \delta_p \max_{k \in p} \frac{D_k}{d_k} + P_f \frac{L_u}{v_f} \right) \tag{18a}$$

$$\text{s.t.} \quad p_{\min} \leq p_k \leq p_{\max}, \qquad \forall k, \tag{18b}$$

$$\sum_{p:k \in p} \delta_p \leq 1, \qquad \forall k, \tag{18c}$$

$$\rho\, p_{i(p)} G_{i(p)} \leq p_{j(p)} G_{j(p)}, \qquad \forall p \in P_{\text{NOMA}}, \tag{18d}$$

$$\frac{p_k G_{k,u(p)}}{\sigma_u^2} \geq \gamma_{\min}, \qquad \forall k \in p,\ \forall p \text{ with } \delta_p = 1, \tag{18e}$$

$$\|\mathbf{q}_u(n+1) - \mathbf{q}_u(n)\| \leq v_{\max}\Delta t, \qquad \forall u,\ \forall n, \tag{18f}$$

$$\mathbf{q}_u(N_u) = \mathbf{q}_u(0), \qquad \forall u, \tag{18g}$$

$$\delta_p \in \{0,1\}, \qquad \forall p \in P. \tag{18h}$$

Constraint (18b) limits the transmit power of each IoT device to its feasible operating range. Constraint (18c) ensures that each device can participate in at most one NOMA pair. Constraint (18d) guarantees the power-domain separation required for successful SIC decoding, where $i(p)$ and $j(p)$ denote the strong and weak users in pair p, respectively. Constraint (18e) enforces the minimum SNR requirement needed for reliable uplink decoding at the UAV. Constraint (18f) ensures physically feasible UAV motion by restricting the maximum displacement between successive hovering points according to the UAV speed limit $v_{\max}$. Constraint (18g) requires each UAV to complete a closed trajectory. Constraint (18h) specifies the binary nature of the pairing decision variables.

Due to the intrinsic coupling among the discrete pairing variables, the continuous transmit-power variables, and the UAV trajectory variables, problem $\mathcal{P}_1$ is a mixed-integer nonlinear program (MINLP), which is generally NP-hard and computationally intractable to solve optimally.

After completing the IoT data-collection stage, each UAV proceeds to offload its aggregated task data to LEO satellites. The objective of the second-stage decision process is to minimize unnecessary handover events while guaranteeing the required offloading throughput. This improves QoS continuity and implicitly reduces both transmission and handover-related energy consumption.

The handover-aware satellite association problem is formulated as

$$\mathcal{P}_2 : \min_{\mathbf{x}} \quad \sum_{u=1}^{U} \sum_{t=1}^{T} h_{u,t} \tag{19a}$$

$$\text{s.t.} \quad \sum_{s=1}^{S} \sum_{t=1}^{T} x_{s,u,t} d_{s,u,t} \Delta t \geq D_u, \qquad \forall u, \tag{19b}$$

$$\sum_{s=1}^{S} x_{s,u,t} \leq 1, \qquad \forall u, \forall t, \tag{19c}$$

$$x_{s,u,t} \leq a_{s,u,t}, \qquad \forall s, u, t, \tag{19d}$$

$$\sum_{s=1}^{S} \sum_{t'=t}^{T} x_{s,u,t'} d_{s,u,t'} \Delta t \geq D_u^{\text{rem}}(t), \qquad \forall u, \forall t, \tag{19e}$$

$$x_{s,u,t} \in \{0,1\}, \qquad \forall s, u, t. \tag{19f}$$

Constraint (19b) ensures that the total successfully offloaded data meets the UAV's task requirement. Constraint (19c) restricts each UAV to associate with at most one satellite at each time slot. Constraint (19d) guarantees that association is allowed only when the satellite satisfies the minimum elevation angle, where $a_{s,u,t} \in \{0,1\}$ denotes the satellite visibility indicator, with $a_{s,u,t} = 1$ if $\theta_{s,u,t} \geq \theta_{\min}$ and $a_{s,u,t} = 0$ otherwise. Constraint (19e) avoids unnecessary switching by ensuring that the currently selected satellite can meet the remaining offloading demand under the predicted link evolution, where $D_u^{\text{rem}}(t)$ denotes the remaining data to be uploaded at time t. Constraint (19f) specifies the binary nature of the association decisions.

Due to the temporal coupling of the binary association variables and the predicted throughput evolution, problem $\mathcal{P}_2$ is combinatorial and generally NP-hard. Thus, instead of computing the exact optimal solution, a demand-aware handover strategy is developed to obtain a practically efficient association policy.

3. ALGORITHM DESIGN

To efficiently solve the joint IoT–UAV data collection and UAV–LEO offloading problem, the proposed framework adopts a two-stage hierarchical design. In the first stage,

corresponding to the IoT-to-UAV data transmission process, Algorithm 1 performs pair-based user grouping, transmit-power allocation, and UAV trajectory planning to minimize the UAV energy consumption. In the second stage, associated with the UAV-to-LEO offloading process, Algorithm 2 executes a demand-aware satellite selection strategy that mitigates unnecessary handovers while ensuring the required offloading throughput and QoS continuity.

3.1. UAV Data Collection and Energy Optimization

To effectively solve problem $\mathcal{P}_1$, we focus on minimizing the total UAV energy consumption incurred during the IoT–UAV data collection stage. Since the communication energy of IoT devices is negligible compared to the hovering and flight energy of UAVs, the optimization primarily targets the UAV energy components. The decision variables include the discrete pair-selection indicators $\delta = \{\delta_p \mid p \in P\}$, the continuous transmit-power allocation $\mathbf{p} = \{p_k \mid k \in K\}$, and the UAV hovering positions $\mathbf{q} = \{\mathbf{q}_u(n) \mid u \in U\}$.

The resulting problem is a MINLP characterized by tight coupling among discrete pairing decisions, continuous power variables, and geometric trajectory variables, making it computationally intractable to solve optimally. To address this challenge, we develop an alternating-optimization framework enhanced with a local-search refinement procedure. The overall algorithmic workflow is illustrated in Fig. 3 and summarized in Algorithm 1.

The initial NOMA pairs are formed using a distance-based greedy strategy. The pairwise distance matrix of all IoT devices is first computed, and the two closest devices that satisfy the NOMA feasibility constraints are grouped into a pair and added to the pair set P. This procedure is repeated until no additional valid pairs can be formed, and any remaining devices are treated as independent OFDMA users.

For each activated NOMA pair $p \in P$ with $\delta_p = 1$, an alternating-optimization procedure is executed to jointly refine the power allocation and UAV hovering position. Given a fixed UAV position (x_u, y_u, h_u), the transmit powers of the paired devices are updated using a block coordinate descent (BCD) approach. Specifically, for each NOMA pair p, the transmit power of one user in p is updated via a Newton-type step while the power of the other user is kept fixed, followed by a projection onto the feasible power domain to satisfy the NOMA decoding constraints. This process repeats until convergence. For OFDMA users, the transmit power is directly set to $p_{\max}$ to maximize the throughput and reduce hovering time.

With the power allocation fixed, the UAV hovering point (x_u, y_u) ,where altitude h_u kept constant, is refined using the Adam optimizer, which leverages momentum and adaptive learning rates to accelerate convergence compared with gradient-free heuristics. The update rule is

$$\mathbf{m}_t = \beta_1 \mathbf{m}_{t-1} + (1 - \beta_1)\nabla_{\mathbf{q}} E_{\text{total}}, \tag{20}$$

$$\mathbf{v}_t = \beta_2 \mathbf{v}_{t-1} + (1 - \beta_2)(\nabla_{\mathbf{q}} E_{\text{total}})^2, \tag{21}$$

$$\mathbf{q}_u^{(t+1)} = \mathbf{q}_u^{(t)} - \alpha \frac{\hat{\mathbf{m}}_t}{\sqrt{\hat{\mathbf{v}}_t} + \epsilon}, \tag{22}$$

where $\mathbf{m}_t$ and $\mathbf{v}_t$ denote the first- and second-order moment estimates, and α, β_1, and β_2 are the learning-rate and decay parameters, respectively. The alternating procedure iterates until reaching the maximum iteration count J or until the reduction in objective value falls below a predefined threshold.

After determining all UAV hovering positions, the visiting order must be optimized to minimize the total flight distance. This routing subproblem is a variant of the multiple traveling salesman problem (mTSP). To refine the trajectory, the 2-opt local search algorithm is employed. In each iteration, two edges in the current tour are removed and reconnected
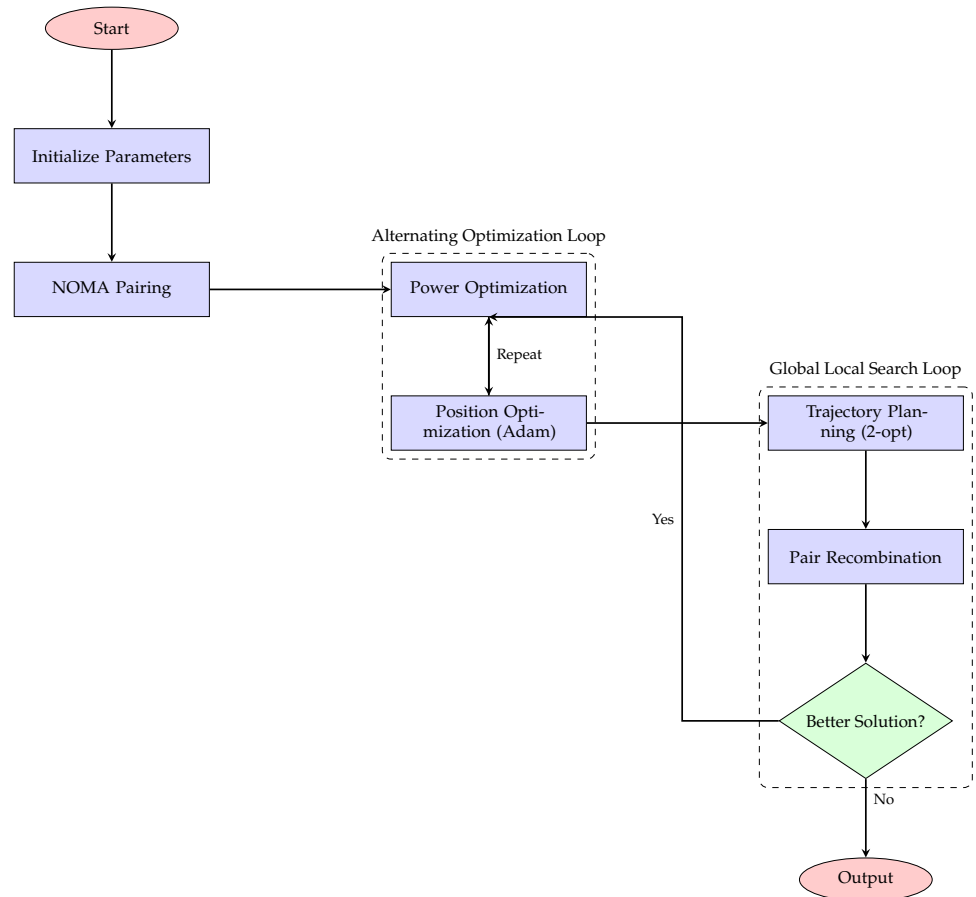
Figure 3. Flowchart of the proposed UAV data collection algorithm with NOMA pairing, power control, and trajectory optimization.

in an alternative configuration. If the resulting trajectory shortens the total travel distance and eliminates path crossings, the update is accepted. The procedure is repeated until no further improvement is possible. Compared with metaheuristic approaches, 2-opt offers faster convergence and more stable performance for trajectory refinement in mTSP settings.

To further reduce energy consumption, a pair-recombination mechanism is introduced to enhance the NOMA pairing structure. Each unpaired device is examined to identify opportunities for forming a new NOMA pair with a member of an existing pair, provided that the resulting pair satisfies the NOMA decoding feasibility conditions. Similarly, for two spatially adjacent NOMA pairs, their members are evaluated for potential exchange if such a swap can reduce either UAV flight distance or hovering time while preserving NOMA constraints.

After each recombination or exchange operation, the UAV trajectory and the corresponding total energy consumption are recalculated. A new configuration is accepted only if it yields a strictly lower energy value; otherwise, the previous configuration is retained. By iteratively applying trajectory refinement and pairing-structure updates, the algorithm explores a broader solution space and achieves improved NOMA pairing and flight-path configurations. The full procedure is summarized in Algorithm 1, with the corresponding flowchart shown in Fig. 3.

3.2. LEO Satellite Selection Optimization

After completing the data collection phase, the UAV must offload its aggregated information to LEO satellites for further processing. In contrast to stationary terrestrial ground stations, LEO satellites move rapidly along predetermined orbital trajectories,

---

Algorithm 1 UAV Data Collection and Energy Optimization

1: **Input:** IoT device locations $\{\mathbf{q}_k\}$, data sizes $\{D_k\}$, UAV initial position $\mathbf{q}_u(0)$
2: **Output:** Total energy consumption E_{total}
                 ▷ Stage 1: Initial NOMA Pairing
3: Construct the distance matrix of all IoT devices
4: Form the initial NOMA pair set P using distance-based greedy pairing
5: Let U_{solo} be the set of unpaired devices
            ▷ Stage 2: Alternating Optimization (Power ↔ Position)
6: Initialize UAV hovering position $\mathbf{q}_u$
7: Initialize transmit-power vector $\mathbf{p}$
8: **for** $j = 1$ to J **do**
9:   Update $\mathbf{p}$ via Newton-type block coordinate descent with projection onto feasible power and NOMA constraints
10:   Update UAV hovering position $\mathbf{q}_u$ using the Adam optimizer
11: **end for**
                   ▷ Stage 3: Trajectory Optimization
12: Generate an initial visiting order for all UAV hovering waypoints
13: Refine the trajectory using the 2-opt local search algorithm
14: Compute the initial total energy E_{total} using (18a)
           ▷ Stage 4: Global Local Search with Pair Recombination
15: **repeat**
16: *improved* ← **false**
17: **for** each NOMA pair $p \in P$ **do**
18:   **for** each unpaired device $k \in U_{\text{solo}}$ **do**
19:    Propose a recombination or user exchange between k and pair p
20:    **if** the new pairing satisfies NOMA decoding constraints **then**
21:     Re-run Stage 2 (power and position optimization)
22:     Re-run Stage 3 (trajectory refinement)
23:     Compute updated energy E_{new}
24:     **if** $E_{\text{new}} < E_{\text{total}}$ **then**
25:      Accept the new configuration
26:      $E_{\text{total}} \leftarrow E_{\text{new}}$
27:      *improved* ← **true**
28:     **else**
29:      Reject the new configuration and revert to the previous one
30:     **end if**
31:    **end if**
32:   **end for**
33: **end for**
34: **until** *improved* = **false**
35: **return** E_{total}

---

resulting in highly time-varying channel conditions and limited visibility windows. As a result, the satellite association decision plays a critical role in determining both the achievable uplink throughput and the stability of the communication link.

Frequent satellite handovers lead to increased signaling overhead, potential packet loss, and service interruptions, thereby degrading the overall quality of service. On the other hand, maintaining a connection to a satellite with deteriorating link quality prolongs transmission time and increases energy consumption. Hence, an effective association strategy must carefully balance the tradeoff between reducing unnecessary handovers and preserving sufficient link quality to ensure timely and reliable data offloading.

To address problem $\mathcal{P}_2$, a demand-aware satellite selection mechanism is proposed. Instead of adopting a greedy policy that always associates with the satellite providing the highest instantaneous throughput, the proposed algorithm assesses whether the currently connected satellite can still satisfy the remaining offloading demand based on the predicted
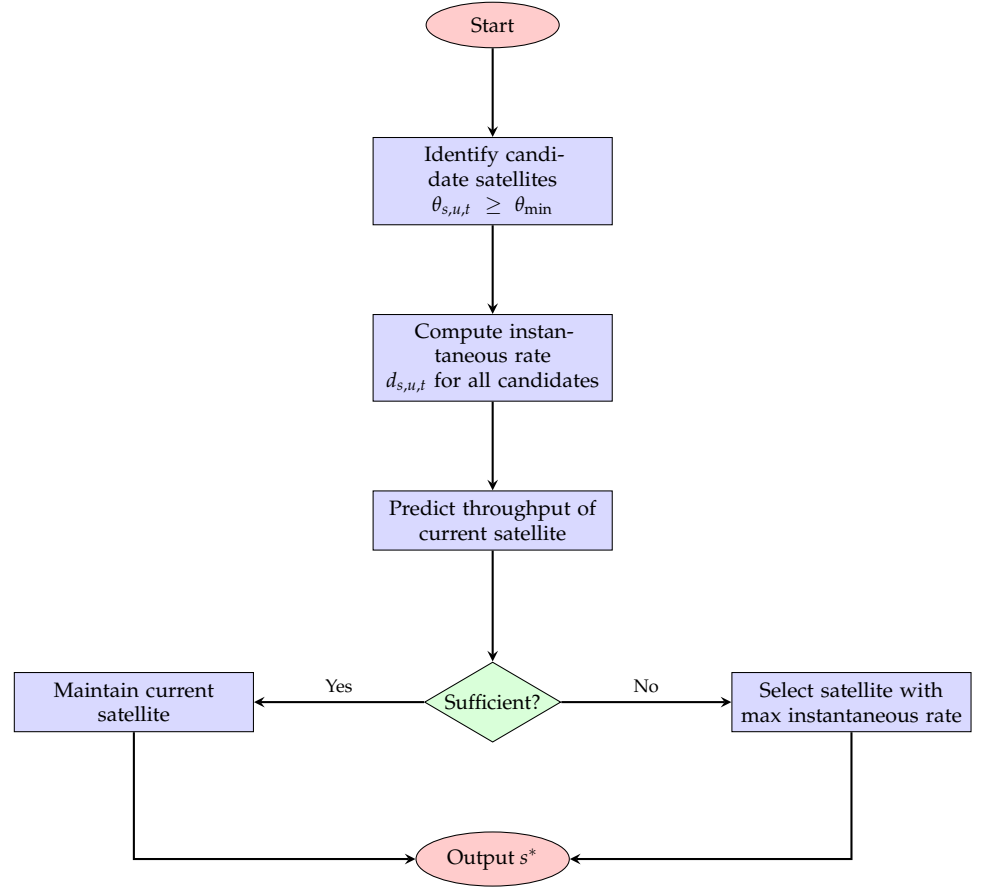
Figure 4. Flowchart of the demand-aware LEO satellite selection algorithm.

link evolution. A handover is triggered only when the projected achievable throughput of the current link becomes insufficient to complete the remaining task, thereby avoiding unnecessary switching while ensuring timely and reliable data delivery.

At each decision epoch, all LEO satellites satisfying the elevation constraint $\theta_{s,u,t} \geq \theta_{\min}$ are identified as candidate satellites. For each candidate s, the instantaneous uplink rate $d_{s,u,t}$ is computed using (16) based on the distance-dependent channel gain. The algorithm then predicts the cumulative throughput that the currently associated satellite can provide over its remaining visibility window. If this predicted throughput exceeds the remaining data requirement $D_u^{\text{rem}}(t)$, the current association is maintained. Otherwise, a handover is initiated to the candidate satellite offering the maximum instantaneous throughput.

4. SIMULATION RESULTS

The performance of the proposed two-stage optimization framework is evaluated through extensive simulations. The first stage focuses on UAV-assisted IoT data collection, whereas the second stage considers LEO satellite offloading. All simulation parameters used in these two stages are summarized in Tables 1 and 2, respectively. The experiments are implemented in Python 3.10 on a workstation equipped with an Intel Core i7-12700K CPU and 32 GB RAM.

The first part of the evaluation focuses on the ground-to-air segment. A fixed-altitude UAV operates within a 500×500 m^2 area containing spatially distributed IoT devices, reflecting typical low-altitude urban deployments. Each scenario is executed under three independent random seeds, and results are averaged. To evaluate the effectiveness of the proposed Adam-2opt algorithm, three baseline strategies are considered

Table 1. Simulation parameters for the UAV-assisted IoT data collection stage.

Parameter	Value	Parameter	Value
K (IoT devices)	20	N (hover points)	10
D_k (data size)	10 MB	B_{iu}	1 MHz
$P_{\max}$	5 W	$P_{\min}$	0.1 W
P_h	100 W	P_f	150 W
v_f	10 m/s	h_u	100 m
β_0	10^{-5}	σ_{iu}^2	10^{-9} W
ρ	0.8	$d_{\max}$	100 m
Area size	500×500 m^2	α (Adam)	0.01
β_1 (Adam)	0.9	β_2 (Adam)	0.999
J (max iterations)	100	ϵ	10^{-6}

Table 2. Communication and orbital parameters for the LEO satellite offloading stage.

Parameter	Value	Parameter	Value
$\theta_{\min}$	15°	B_{su}	10 MHz
P_{tr}	10 W	G_{tr}	10 dBi
G_{re}	30 dBi	σ_{su}^2	4×10^{-14} W
f_s	20 GHz	r_e	6378 km
h_s (LEO altitude)	550 km	ω_E	7.29 rad/s
Constellation	Starlink	Num. satellites	200
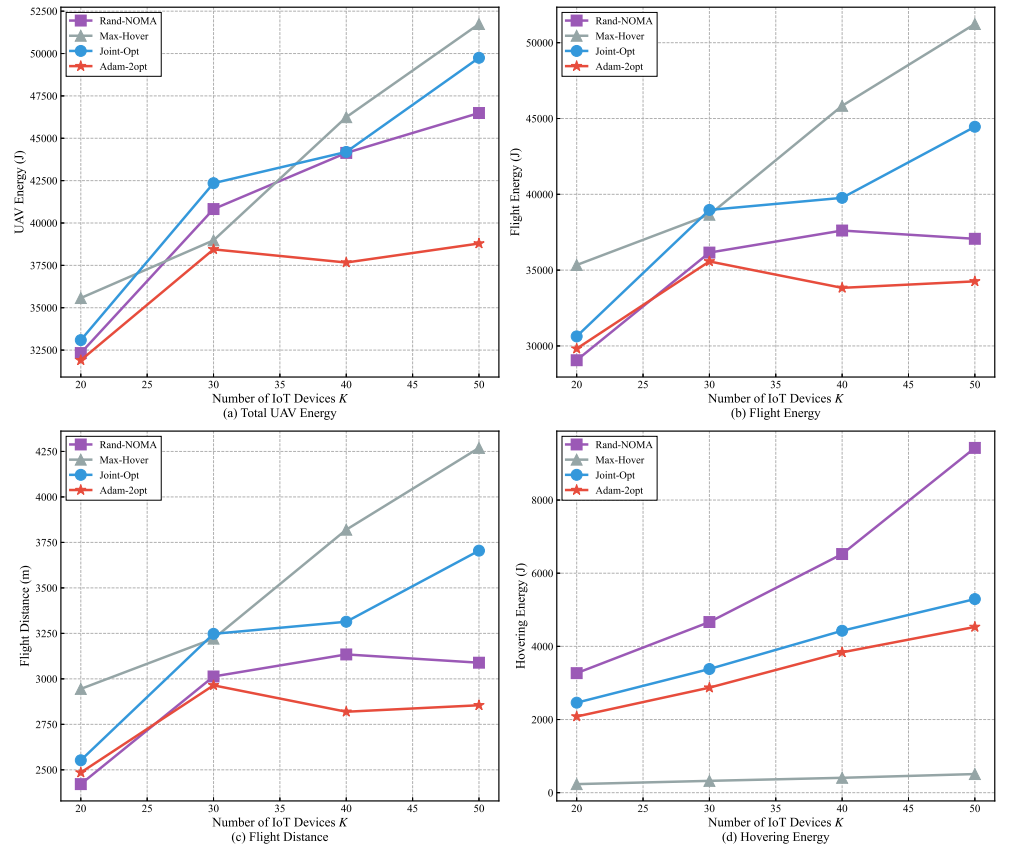
Figure 5. Performance comparison of four algorithms—Random Pairing, Fixed Hovering, Basic Optimization, and Adam-2opt—in the IoT–UAV data collection stage across energy and trajectory metrics.

Algorithm 2 Demand-Aware LEO Satellite Selection

1: **Input:** UAV position $\mathbf{q}_u(t)$, total data size D_u, transmitted data D_u^{tx}, current satellite s_{curr}, current time t
2: **Output:** Selected satellite s^*
3: Compute remaining data $D_u^{\text{rem}}(t) \leftarrow D_u - D_u^{\text{tx}}$
4: Initialize candidate set $\mathcal{S}_{\text{cand}} \leftarrow \varnothing$
5: **for** each satellite $s \in \mathcal{S}$ **do**
6:      Compute elevation angle $\theta_{s,u,t}$ using (13)
7:      **if** $\theta_{s,u,t} \geq \theta_{\min}$ **then**
8:          $\mathcal{S}_{\text{cand}} \leftarrow \mathcal{S}_{\text{cand}} \cup \{s\}$
9:      **end if**
10: **end for**
11: **if** $s_{\text{curr}} \in \mathcal{S}_{\text{cand}}$ **then**
12:      Predict visibility window end time $t_{\text{exit}}(s_{\text{curr}})$
13:      $T_{\text{vis}} \leftarrow t_{\text{exit}}(s_{\text{curr}}) - t$
14:      Predict future achievable throughput:

$$\hat{D}_{\text{curr}} \leftarrow \sum_{t'=t}^{t_{\text{exit}}} d_{s_{\text{curr}},u,t'} \Delta t$$

15:      **if** $\hat{D}_{\text{curr}} \geq D_u^{\text{rem}}(t)$ **then**
16:          **return** s_{curr} ▷ Current link sufficient, no handover
17:      **end if**
18: **end if**
19: Choose the best candidate:

$$s^* \leftarrow \arg\max_{s \in \mathcal{S}_{\text{cand}}} d_{s,u,t}$$

20: **return** s^*

- *Random Pairing*: forms NOMA pairs without channel awareness.
- *Fixed Hovering*: minimizes hovering duration but does not optimize flight paths.
- *Basic Optimization*: performs pairing, power allocation, and position refinement but lacks trajectory planning.

The second part of the evaluation focuses on the air-to-space offloading stage. A Starlink constellation at 550 km altitude is simulated, where the number of visible satellites varies over time due to orbital dynamics. The UAV employs a 20 GHz carrier frequency and is subject to a minimum elevation-angle constraint when establishing a satellite link. Each handover event incurs a fixed 400 ms interruption. A 10-minute evaluation window with 20-second time resolution is considered, during which multiple handover opportunities arise.

Two satellite-selection strategies are compared

- *Greedy*: always associates with the satellite providing the highest instantaneous rate.
- *Demand-Aware*: triggers handover only when the predicted throughput of the current link becomes insufficient to meet the remaining offloading demand.

4.1. Ground-to-Air Data Acquisition Performance

The ground-to-air data acquisition stage poses a tightly coupled optimization problem involving NOMA pairing, power allocation, and UAV trajectory design. Figure 5 summarizes the performance of all evaluated algorithms across four key metrics. The results consistently show that the proposed Adam-2opt method delivers the most energy-efficient operation, particularly in dense IoT deployments.We now analyze the performance differences across the four metrics and relate them to the algorithmic properties of each method.
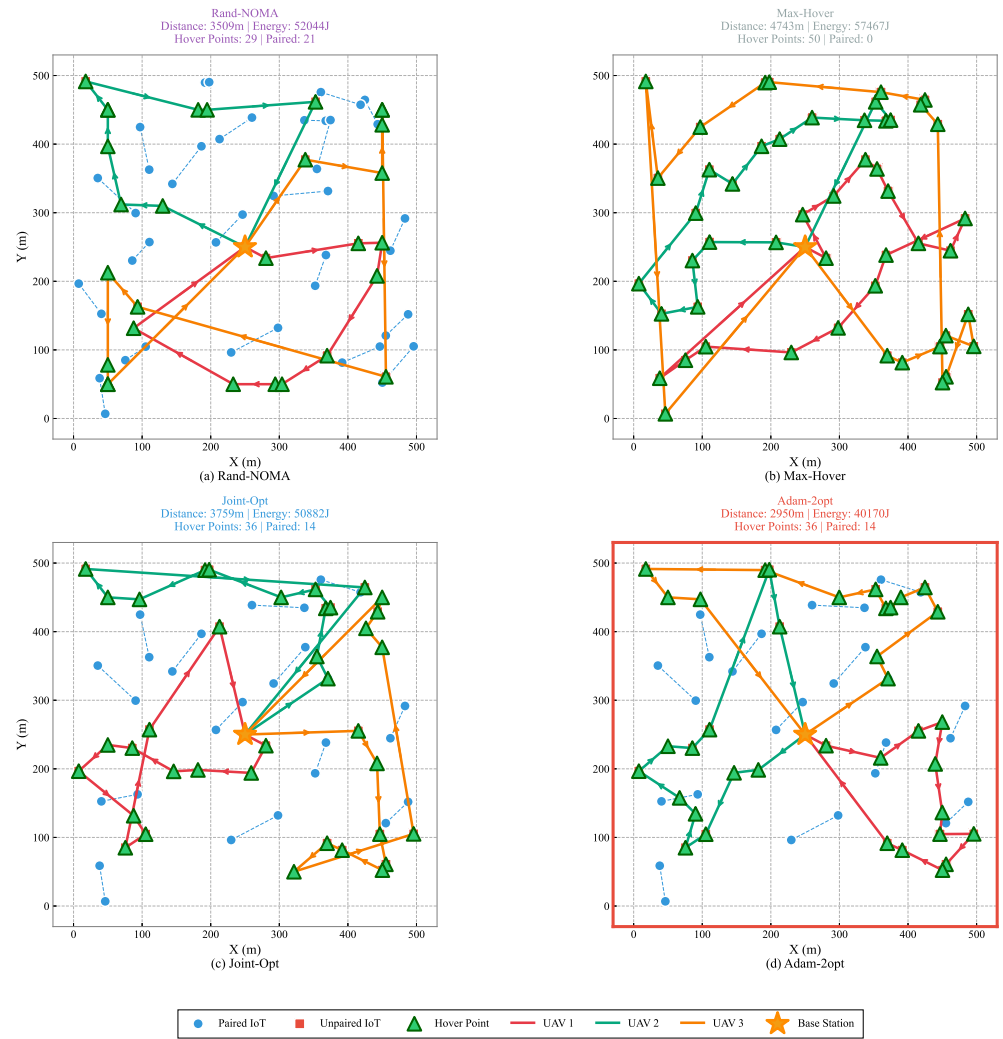
Figure 6. UAV trajectory comparison between different optimization algorithms.

Figure 5a indicates that total UAV energy consumption increases with the number of IoT devices, yet the proposed method exhibits the slowest growth trend. While all algorithms perform similarly under low-density conditions ($K = 20$), the performance gap widens significantly as the network scales. At $K = 50$, Adam-2opt achieves more than 16% energy reduction compared with Random Pairing, and over 22% compared with Basic Optimization. This demonstrates that advanced trajectory refinement becomes increasingly valuable when device clustering and route complexity intensify.

The primary advantage of Adam-2opt arises from its ability to simultaneously optimize hovering locations and visit sequencing. As shown in Figure 5c, the proposed design produces the shortest flight distance among all methods, with a reduction exceeding 30% relative to Fixed Hovering at high densities. The 2-opt refinement eliminates path crossings and unnecessary detours, which directly translates into reduced flight energy, as reflected in Figure 5b. These improvements highlight the importance of trajectory-level optimization in UAV-assisted data collection.

Hovering energy behavior, depicted in Figure 5d, provides additional insight into algorithmic trade-offs. Fixed Hovering minimizes hovering time by construction but suffers from excessive flight distance, leading to the highest overall energy consumption. Random Pairing exhibits the opposite issue: arbitrary device grouping produces spatially dispersed clusters, substantially increasing hovering duration. By contrast, Adam-2opt maintains balanced performance—hovering time is reduced by nearly 50% compared with Random Pairing—while preserving the shortest flight trajectory. This balanced design is essential for missions where both hovering and flight energy dominate total consumption.

To further illustrate spatial efficiency, Figure 6 visualizes representative flight paths for $K = 50$. The Random Pairing trajectory in Figure 6a exhibits numerous path crossings and backtracking segments, reflecting the inherently unstructured nature of its device grouping. Fixed Hovering in Figure 6b generates uniformly distributed hovering points; however, the resulting path forces UAVs to traverse many redundant transitions, leading to substantially increased flight distance. Basic Optimization in Figure 6c improves spatial locality but still retains avoidable turns and several suboptimal visiting sequences. In contrast, the proposed Adam-2opt trajectory in Figure 6d is markedly more compact and well organized, exhibiting no path intersections and maintaining a coherent directional pattern. These observations confirm the complementary roles of Adam-based hovering refinement and 2-opt sequencing in producing globally efficient UAV flight paths.

Computational cost results indicate that Adam-2opt incurs higher planning time due to its iterative refinement steps. Nevertheless, the total runtime remains on the order of one second—negligible for offline mission planning. Given that the resulting energy savings exceed 16% in dense deployments, the computational overhead is well justified and supports the practicality of the proposed approach for pre-scheduled UAV operations.

Finally, the scalability trends observed in Figure 5 highlight an important system-level implication. Whereas simple heuristics maintain acceptable performance in small networks, their efficiency degrades rapidly as the device density increases. In contrast, Adam-2opt demonstrates sublinear growth in energy consumption and maintains robust performance as K scales upward. These results suggest that the proposed framework is particularly well suited for large-scale IoT deployments, where spatial clustering and route complexity necessitate more sophisticated optimization mechanisms.

4.2. UAV–LEO Offloading Performance

The second stage evaluates the offloading of aggregated data from UAVs to LEO satellites, where the dominant challenge shifts from spatial optimization to coping with highly time-varying satellite visibility. Unlike the ground-to-air segment, the air-to-space

link is governed by rapid orbital motion, causing frequent changes in elevation angle, link quality, and service continuity. As a result, maintaining a stable connection becomes as critical as achieving high instantaneous throughput, motivating the need for intelligent and demand-aware handover strategies.
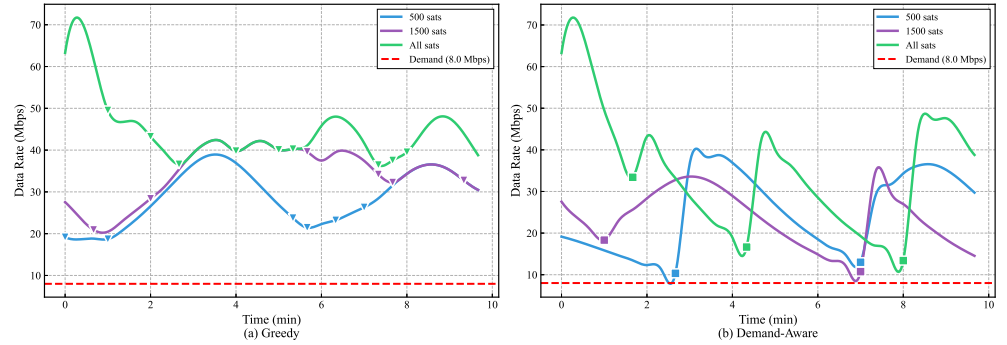
Figure 7. Data rate trajectories of Greedy and Demand-Aware satellite selection strategies for different LEO constellation sizes.

A key observation from Figure 7 is the fundamental difference in handover behavior between the two evaluated strategies. The Greedy scheme continually switches to the satellite offering the highest instantaneous rate, resulting in pronounced rate volatility and frequent handover events. This behavior becomes more severe as satellite density increases, reflecting its sensitivity to instantaneous channel variations rather than long-term transmission feasibility.

In contrast, the Demand-Aware strategy produces consistently smoother rate trajectories and dramatically fewer handovers. By maintaining the current satellite connection as long as the remaining data demand can be satisfied within the predicted visibility window, the method avoids unnecessary switching and preserves link continuity. This design principle leads to a stable operating regime across all constellation densities, with only two to three handovers observed even in large constellations. Figure 8a quantitatively
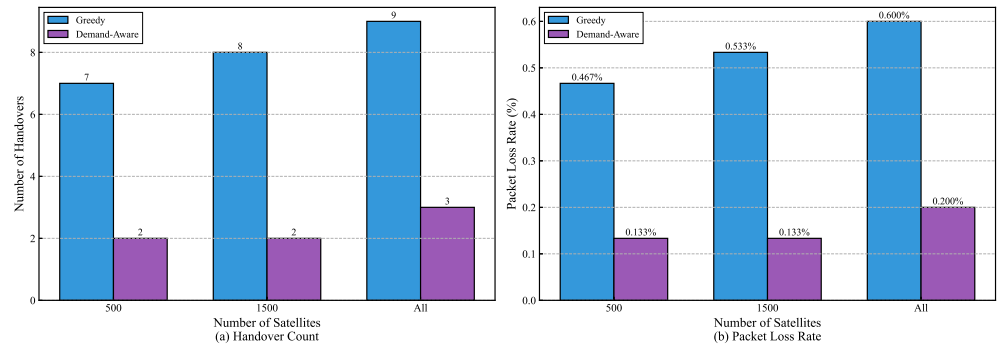
Figure 8. Comparison of handover frequency and packet loss rate for Greedy and Demand-Aware satellite selection strategies under different constellation sizes.

highlights this stability. Demand-Aware consistently reduces handover occurrences by 66–75% relative to Greedy, and the reduction remains nearly invariant across the 500-, 1500-, and full-constellation scenarios. This invariance is particularly notable because it shows that the strategy scales gracefully with constellation size: the number of available satellites increases, but the handover count does not. Thus, Demand-Aware does not exploit satellite density to switch more frequently; instead, it leverages it to sustain longer, more reliable connections.

The practical implication of reduced handover activity is evident in the packet loss performance shown in Figure 8b. Because every handover incurs a fixed interruption period,

lower switching frequency directly translates into proportionally lower loss rates. Demand-Aware maintains packet loss between 0.133% and 0.200%, whereas Greedy experiences losses three to four times higher. Although the absolute percentages appear small, the difference corresponds to several tens of kilobits over a typical mission—non-negligible for latency-sensitive applications such as real-time sensing or video uplink. These results demonstrate that optimizing for stability can yield a more reliable offloading process than purely maximizing instantaneous rate.

A trade-off emerges when examining average throughput. The Greedy strategy attains higher mean rates due to its aggressive switching behavior; however, this throughput advantage comes at the cost of substantial instability, packet loss, and service disruption. Demand-Aware yields 13–32% lower average rates, but still consistently exceeds the required 8 Mbps demand by a comfortable margin. This surplus indicates that the system is operating well above its QoS threshold even without chasing maximum instantaneous rate, validating that rate maximization is not the limiting factor in this stage.

Finally, the scalability behavior across constellations provides insight into future LEO deployments. As the density of satellites increases, Greedy becomes increasingly unstable, with handover counts rising due to more frequent rate fluctuations. Demand-Aware, however, maintains nearly identical performance across all densities. This robustness arises from its demand-driven decision rule, which depends on the time required to complete the remaining offloading task rather than on short-term channel variations. Consequently, the method remains effective even as constellation sizes grow, making it well-suited for next-generation, high-density LEO systems.

4.3. End-to-End System Analysis

To assess the system-wide benefits of the proposed two-stage framework, we evaluate the total mission energy consumption—including IoT uplink transmission, UAV propulsion, and LEO-side processing—summarized in Figure **??**. This metric captures the cumulative effect of both spatial optimization during data acquisition and temporal stability during satellite offloading.

The results demonstrate a clear and consistent improvement over the baseline strategies. The Adam-2opt method reduces flight distance and hovering duration, thereby lowering the dominant propulsion energy in the acquisition stage. These savings directly translate into a shorter collection phase and a more structured aggregated data load. As a result, the Demand-Aware offloading stage operates under reduced temporal pressure, requiring fewer handovers and avoiding retransmissions. This stability further suppresses unnecessary communication energy on both the UAV and satellite sides.

Figure **??** shows that the combined Adam-2opt + Demand-Aware pipeline achieves approximately 8–12% lower total mission energy compared with the baselines. Importantly, these reductions do not arise from a single component but reflect the complementary function of both stages: Algorithm 1 minimizes the work that Algorithm 2 must perform under rapidly varying link conditions, while Algorithm 2 ensures reliable and interruption-free delivery of the data produced by Algorithm 1.

Overall, the end-to-end evaluation confirms that optimizing spatial and temporal dimensions jointly yields significantly better system-level performance than optimizing either stage in isolation. By aligning trajectory planning with demand-aware offloading control, the proposed framework provides a robust and energy-efficient solution for UAV–LEO integrated operations.

5. Discussion

The simulation results reveal several broader insights that extend beyond individual algorithmic performance and speak to the design of integrated UAV–LEO systems. A first overarching finding is that spatial efficiency in the ground segment and temporal stability in the space segment must be treated as complementary objectives rather than independent concerns. The two-stage results clearly show that trajectory refinement not only reduces propulsion energy but also produces a more predictable data acquisition window, which in turn enables stable and interruption-free satellite offloading.

The end-to-end experiment further reinforces this interaction. By jointly considering IoT transmission, UAV propulsion, and LEO processing energy, Figure **??** demonstrates that the Adam-2opt + Demand-Aware pipeline consistently lowers total mission cost compared with baseline strategies. These reductions arise from distinct but mutually reinforcing mechanisms: Algorithm 1 suppresses spatial redundancy, while Algorithm 2 minimizes temporal disruptions by avoiding unnecessary handovers. The combined effect illustrates that system-level gains emerge not from aggressively optimizing a single stage, but from aligning optimization principles across stages.

Another key insight concerns the shift from instantaneous-performance objectives toward sufficiency-based decision making in the satellite segment. The Demand-Aware strategy demonstrates that maximizing short-term throughput is neither necessary nor desirable in dynamic LEO environments. Instead, ensuring link continuity—so long as rate is sufficient to meet the remaining demand—reduces switching overhead, packet loss, and retransmissions. This reframing suggests that future SAGIN handover mechanisms should prioritize mission-level guarantees rather than instantaneous signal metrics.

The results also highlight why a fully integrated UAV–LEO optimization framework is neither practical nor advantageous. The two processes operate on fundamentally different temporal scales: UAV trajectories evolve on minute-level horizons with predictable spatial geometry, whereas satellite visibility varies on the order of seconds. Attempting to couple these dynamics in a single monolithic optimization would either overwhelm the trajectory planner or slow down the handover controller beyond usability. The proposed two-stage decomposition is therefore not merely a computational simplification, but an architectural necessity dictated by heterogeneous system dynamics.

Finally, the scalability trends emphasize the robustness of this decomposition. As IoT density increases, the benefits of spatial optimization grow more pronounced, while the Demand-Aware handover rule maintains nearly invariant behavior across satellite densities. These properties suggest that modular, stage-aligned optimization is particularly well suited for future large-scale SAGIN deployments. Nonetheless, real-world implementations will require accounting for uncertainties in device mobility, channel estimation errors, and asynchronous multi-UAV coordination—factors that offer promising directions for extending the present framework.

6. Conclusions

This work presented a two-stage optimization framework that integrates energy-efficient UAV trajectory planning with stability-oriented LEO satellite offloading for SAGIN-based IoT collection. By aligning spatial and temporal optimization principles, the framework achieves reliable and energy-efficient end-to-end performance without requiring computationally prohibitive joint optimization. The results demonstrate strong scalability with respect to both IoT device density and satellite constellation size, underscoring the practicality of the proposed approach for next-generation aerial–satellite IoT systems. Future work may extend the framework to uncertainty-aware trajectory control and cooperative multi-UAV offloading, further enhancing robustness in real-world deployments.

References

1. Jia, Z.; Sheng, M.; Li, J.; Niyato, D.; Han, Z. LEO-satellite-assisted UAV: Joint trajectory and data collection for Internet of Remote Things in 6G aerial access networks. *IEEE Internet Things J.* **2020**, *8*, 9814–9826.

2. Xiao, Y.; Ye, Z.; Wu, M.; Li, H.; Xiao, M.; Alouini, M.-S.; Al-Hourani, A.; Cioni, S. Space-air-ground integrated wireless networks for 6G: Basics, key technologies and future trends. *IEEE J. Sel. Areas Commun.* **2024**.

3. Duan, S.; Wang, D.; Ren, J.; Lyu, F.; Zhang, Y.; Wu, H.; Shen, X. Distributed artificial intelligence empowered by end-edge-cloud computing: A survey. *IEEE Commun. Surv. Tutor.* **2022**, *25*, 591–624.

4. Wei, Q.; Chen, Y.; Jia, Z.; Bai, W.; Pei, T.; Wu, Q. Energy-efficient caching and user selection for resource-limited SAGINs in emergency communications. *IEEE Trans. Commun.* **2024**.

5. Pan, G.; Ye, J.; An, J.; Alouini, M.-S. Latency versus reliability in LEO mega-constellations: Terrestrial, aerial, or space relay? *IEEE Trans. Mob. Comput.* **2022**, *22*, 5330–5345.

6. Jia, Z.; Cui, C.; Dong, C.; Wu, Q.; Ling, Z.; Niyato, D.; Han, Z. Distributionally robust optimization for aerial multi-access edge computing via cooperation of UAVs and HAPs. *IEEE Trans. Mob. Comput.* **2025**.

7. Mao, S.; He, S.; Wu, J. Joint UAV position optimization and resource scheduling in space-air-ground integrated networks with mixed cloud-edge computing. *IEEE Syst. J.* **2020**, *15*, 3992–4002.

8. Zhao, C.; Liu, J.; Sheng, M.; Teng, W.; Zheng, Y.; Li, J. Multi-UAV trajectory planning for energy-efficient content coverage: A decentralized learning-based approach. *IEEE J. Sel. Areas Commun.* **2021**, *39*, 3193–3207.

9. Mozaffari, M.; Saad, W.; Bennis, M.; Nam, Y.-H.; Debbah, M. A tutorial on UAVs for wireless networks: Applications, challenges, and open problems. *IEEE Commun. Surv. Tutor.* **2019**, *21*, 2334–2360.

10. Tao, Y.; Liu, L.; Liu, S.; Zhang, Z. A survey: Several technologies of non-orthogonal transmission for 5G. *China Commun.* **2015**, *12*, 1–15.

11. Fang, X.; Feng, W.; Wang, Y.; Chen, Y.; Ge, N.; Ding, Z.; Zhu, H. NOMA-based hybrid satellite-UAV-terrestrial networks for 6G maritime coverage. *IEEE Trans. Wireless Commun.* **2022**, *22*, 138–152.

12. Jia, Z.; Cao, Y.; He, L.; Wu, Q.; Zhu, Q.; Niyato, D.; Han, Z. Service function chain dynamic scheduling in space-air-ground integrated networks. *IEEE Trans. Veh. Technol.* **2025**.

13. Xiao, T.; Wang, W.; He, H. Energy-efficient data collection for UAV-assisted IoT: Joint trajectory and resource optimization. *Chin. J. Aeronaut.* **2022**, *35*, 95–105.

14. Wang, B.; Jia, Z.; Cui, C.; Wu, Q. Joint UAV trajectory planning and LEO satellite selection for data offloading in space-air-ground integrated networks. arXiv preprint arXiv:2506.12750 **2025**.

15. Huang, C.; Chen, G.; Xiao, P.; Xiao, Y.; Han, Z.; Chambers, J. A. Joint offloading and resource allocation for hybrid cloud and edge computing in SAGINs: A decision assisted hybrid action space deep reinforcement learning approach. *IEEE J. Sel. Areas Commun.* **2024**, *42*, 1029–1043.

16. Jia, H.; Wang, Y.; Wu, W. Dynamic resource allocation for remote IoT data collection in SAGIN. *IEEE Internet Things J.* **2024**, *11*, 20575–20589.

17. d O Costa, P. R.; Rhuggenaath, J.; Zhang, Y.; Akcay, A. Learning 2-opt heuristics for the traveling salesman problem via deep reinforcement learning. *Asian Conf. Mach. Learn.* **2020**, 465–480.

18. Zhang, H.; Xi, S.; Jiang, H.; Shen, Q.; Shang, B.; Wang, J. Resource allocation and offloading strategy for UAV-assisted LEO satellite edge computing. *Drones* **2023**, *7*, 383.

19. Wang, Y.; Wu, X.; Farooq, J.; Chen, J. Coordinated UAV deployment and task offloading in UAV-assisted LEO satellite edge computing systems via proximal policy optimization. *Authorea Preprints* **2025**.

20. Seyedi, Y.; Rahimi, F. A trace-time framework for prediction of elevation angle over land mobile LEO satellites networks. *Wirel. Pers. Commun.* **2012**, *62*, 793–804.